

Article

# Acidity Suppression of Hole Transport Layer via Solution Reaction of Neutral PEDOT:PSS for Stable Perovskite Photovoltaics

Minseong Kim <sup>1</sup>, Minji Yi <sup>1</sup>, Woongsik Jang <sup>1</sup>, Jung Kyu Kim <sup>2,\*</sup>  and Dong Hwan Wang <sup>1,\*</sup> 

<sup>1</sup> School of Integrative Engineering, Chung-Ang University, Seoul 06974, Korea; kms4587@cau.ac.kr (M.K.); yi4110@cau.ac.kr (M.Y.); dndtlr2@cau.ac.kr (W.J.)

<sup>2</sup> School of Chemical Engineering, Sungkyunkwan University (SKKU), Suwon-si 16419, Korea

\* Correspondence: legkim@skku.edu (J.K.K.); king0401@cau.ac.kr (D.H.W.);  
Tel.: +82-31-290-7254 (J.K.K.); +82-2-820-5074 (D.H.W.)

Received: 27 November 2019; Accepted: 1 January 2020; Published: 6 January 2020



**Abstract:** Poly(3,4-ethylenedioxythiophene): poly(4-styrenesulfonate) (PEDOT:PSS) is typically used for hole transport layers (HTLs), as it exhibits attractive mechanical, electrical properties, and easy processability. However, the intrinsically acidic property can degrade the crystallinity of perovskites, limiting the stability and efficiency of perovskite solar cells (PSCs). In this study, inverted CH<sub>3</sub>NH<sub>3</sub>PbI<sub>3</sub> photovoltaic cells were fabricated with acidity suppressed HTL. We adjusted PEDOT:PSS via a solution reaction of acidic and neutral PEDOT:PSS. And we compared the various pH-controlled HTLs for PSCs devices. The smoothness of the pH-controlled PEDOT:PSS layer was similar to that of acidic PEDOT:PSS-based devices. These layers induced favorable crystallinity of perovskite compared with acidic PEDOT:PSS layers. Furthermore, the enhanced stability of pH optimized PEDOT:PSS-based devices, including the prevention of degradation by a strong acid, allowed the device to retain its power conversion efficiency (PCE) value by maintaining 80% of PCE for approximately 150 h. As a result, the pH-controlled HTL layer fabricated through the solution reaction maintained the surface morphology of the perovskite layer and contributed to the stable operation of PSCs.

**Keywords:** conducting polymers; photovoltaic devices; controlled pH; charge transport; stability

## 1. Introduction

The advances in organic optoelectronics rely on the ability to control various transport properties of devices by controlling the morphology and interface deformation and changing charge carrier density and mobility. Device performance is related to the electrical properties and morphologies of the organic materials used to fabricate the devices [1]. Furthermore, the ability to fabricate ultra-thin films with thicknesses in the nanometer scale and with smooth surfaces is advantageous for the fabrication of laminated structures and applications [2–6]. Among the conducting polymers, the most promising material is poly(3,4-ethylene dioxythiophene) (PEDOT) doped with poly(styrene sulfonate) (PSS) (PEDOT:PSS), which consists of a conducting polythiophene derivative bound to a PSS polyanion [7,8]. Because this polymeric system simultaneously has high electrical conductivity, high mechanical flexibility, and good transparency in the visible range [7–13], it has been widely applied for organic photovoltaics, flexible electrodes, light-emitting diodes, field-effect transistors, and thermoelectric generator [7,14–22].

PEDOT:PSS is intrinsically an acidic and hygroscopic material because of its unique chemical structure and hydrophilicity. The high acidity of PEDOT:PSS, which is the most promising hole transport layer (HTL) material in optoelectronic devices, can corrode indium tin oxide (ITO) electrodes, degrade the perovskite, and deteriorate device performance and stability [9–11,13,23–27]. Previous

approaches to solve this problem include neutralizing acidic PEDOT:PSS by strong bases such as NaOH and KOH or using imidazole as an additive [28–31]. The fabrication of PEDOT:PSS depends on various factors, including the ratio of PSS, concentration of solid contents, colloid gel particle size, and viscosity, which can affect the electronic properties and morphologies in the film. In this context, studying the correlation between morphology, solid additives, and fraction of PSS can solve the problems associated with device application.

The residual acidic agents and proton in acidic PEDOT:PSS causes the problem of deterioration of ITO or top electrode and degradation of the perovskite which leads to a decrease of perovskite crystal quality [27,32]. The high viscosity of neutral PEDOT:PSS leads to unsuitable surface morphology for optoelectronic devices. We propose a convenient and successful approach to suppress the acidic property of PEDOT:PSS, using a simple solution reaction that controls the volume ratio of two PEDOT:PSS solutions, acidic, and neutral PEDOT:PSS. We evaluated the effect of pH of PEDOT:PSS on key features that affect the size of colloidal gel particles (tertiary structure) [33], the morphology of PEDOT:PSS, the perovskite active layer, and electrical properties of perovskite solar cells (PSCs). Our results suggest that the use of PEDOT:PSS using the optimal volume ratio of acidic and neutral PEDOT:PSS can not only improve device stability but can also enhance the polymerization degree of PEDOT and increase perovskite crystallinity.

## 2. Materials and Methods

### 2.1. Material Preparation

Methylammonium iodide ( $\text{CH}_3\text{NH}_3\text{I}$ , Dyesol-Timo Co. Ltd., Seongnam, South Korea), lead iodide ( $\text{PbI}_2$ , 99%, Sigma Aldrich, St. Louis, MO, USA),  $\gamma$ -butyrolactone (GBL, Sigma Aldrich, St. Louis, MO, USA), and dimethyl sulfoxide (DMSO, Sigma Aldrich, St. Louis, MO, USA) were used to prepare the  $\text{CH}_3\text{NH}_3\text{PbI}_3$  ( $\text{MAPbI}_3$ ) precursor. Acidic PEDOT:PSS (AI 4083, Heraeus Company, Hanau, Germany) and neutral PEDOT:PSS (Neutral PEDOT:PSS, Sigma Aldrich, St. Louis, MO, USA) were used as HTLs. Imidazole present in the neutral PEDOT:PSS affects the pH of the HTL solution. PCBM (6,6-phenyl-C70 butyric acid methyl ester)/titanium(VI) isopropoxide ( $\text{TiO}_x$ , Sigma Aldrich, St. Louis, MO, USA) was used as the electron transport layer in PSCs.

### 2.2. Thin Film and Device Fabrication

The PSCs were prepared on ITO substrates, which were cleaned using detergent and underwent sonication in deionized water, acetone, and isopropanol. After exposure of ITO substrates to UV ozone for surface modification, the PEDOT:PSS was spin-coated on the ITO substrates and annealed to fabricate a 30-nm-thick thin film.  $\text{CH}_3\text{NH}_3\text{I}$  and  $\text{PbI}_2$  (1.06:1 mol %) were dissolved in DMSO:GBL (3:7 v/v, molar concentration of  $1.4 \text{ mol L}^{-1}$ ). The  $\text{MAPbI}_3$  solution was spin-coated on the PEDOT:PSS thin film, followed by additional treatment with chlorobenzene. Then, the substrates were placed on a hot plate at  $100^\circ\text{C}$  to fabricate a  $\text{MAPbI}_3$  film with a thickness of 300 nm. The PCBM solution was dissolved in chlorobenzene ( $20 \text{ mg mL}^{-1}$ ) and spin-coated onto the surface of  $\text{MAPbI}_3$  at a thickness of 100 nm. To fabricate a 30-nm-thick PCBM layer, the PCBM solution was dissolved in chlorobenzene ( $20 \text{ mg mL}^{-1}$ ) and spin-coated on the  $\text{MAPbI}_3$  layer. Subsequently, a  $\text{TiO}_x$  layer ( $\sim 10 \text{ nm}$ ) was deposited. Finally, an Ag cathode was deposited by thermal evaporation.

### 2.3. Device Characterization

The pH values of PEDOT:PSS were measured using a pH meter (HANNA instruments, Inc., HI8424, Seoul, South Korea). The zeta radii of different ratios of acidic and neutral PEDOT:PSS were examined using a Malvern Zetasizer ZS90 (ZEN3690) to investigate the particle sizes of PEDOT:PSS in the water of each sample. Fourier transform infrared (FTIR) spectra, collected using horizontal attenuated total reflectance (HATR), were recorded on a NICOLET 6700 IR spectrometer. The electrical properties of the PSCs were measured under air mass 1.5 global illumination (AM 1.5 G) using a

solar simulator (Peccell Technologies, PEC-L01) at an intensity of  $100 \text{ mW cm}^{-2}$ , which was calibrated using a silicon reference cell. The current density–voltage characteristics of the PSCs were measured using ZIVE SP1. After power calibration (ABET Technologies, Inc., LS150, Milford, CT, USA) using a monochromator (Dongwoo Optron Co. Ltd., MonoRa-500i, Gwangju, South Korea), the EQE was measured. The surface morphology and roughness of spin-coated films were examined using an atomic force microscope (AFM) in the noncontact mode (Park NX10) and a scanning electron microscope (SEM) (SIGMA model from Carl Zeiss, Inc., Oberkochen, Germany).

### 3. Results and Discussion

The PEDOT:PSS has the chemical structure and general arrangement [34–36] as shown in Figure 1a. The PEDOT:PSS consists of two ionic bond polymers presented in chemical structure. And when the PEDOT:PSS is deposited as a thin film, as the PEDOT is bonded to PSS chains via Coulomb interactions,  $\pi$ -stacking structure between PEDOT and PSS is induced, which improves hole transport property and conductivity [37,38]. The PEDOT:PSS exhibits strong acidic properties and coating a solution with strong acidic PEDOT:PSS can deteriorate the ITO by penetrating the boundary between the solution and the thin film to promote ion release and impede charge flow [11,27,39–41]. Further, the acidic property of PEDOT:PSS can cause the degradation of the top electrode or perovskite active layer and lead to inferior perovskite crystal quality [9–11,13,24,25]. In this study, we minimized the strong acidic properties of PEDOT:PSS and improved the stability of PSCs by controlling the pH of the PEDOT:PSS solution. By mixing acidic PEDOT:PSS and neutral PEDOT:PSS in an optimal ratio, we verified the efficacy of the PEDOT:PSS solution that can be easily prepared. The pH of acidic PEDOT:PSS is approximately 1–2 and the viscosity is approximately 5–12 mPa s. In addition, the pH of neutral PEDOT:PSS is approximately 5–7, and the viscosity is less than 100 mPa s. As depicted schematically in Figure 1b, pH-controlled PEDOT:PSS solutions were prepared by mixing acidic and neutral PEDOT:PSS in the volume ratios of 1:0 (AN10), 1:1 (AN11), and 1:3 (AN13). By mixing acidic and neutral PEDOT:PSS, the pH of the solution increased, and the resistivity decreased, thus enhancing the stability and efficiency of PSCs.

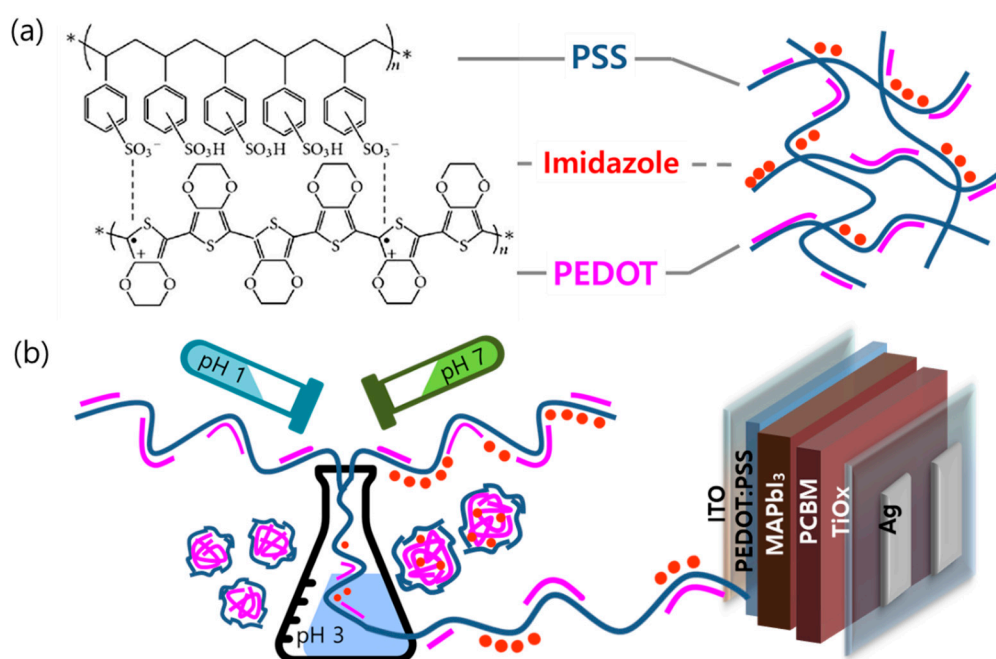


**Figure 1.** (a) Structure and schematic representation of PEDOT:PSS. (b) The solution fabrication process and polymer composite structure of pH-controlled PEDOT:PSS for inverted PSCs.

The PEDOT:PSS consists of gel-like particles containing a PSS<sup>-</sup> shell which stabilizes PEDOT-rich particles in an aqueous solvent [42]. The size of the colloidal PEDOT:PSS gel particle in water is related to the ratio of PEDOT to PSS, as increasing particle size increases the particle boundary surface [33,35,43], see Figure 1b. An increase in the particle size with decreased particle boundaries leads to a few energy barriers which enhance the conductivity of PEDOT:PSS [44,45]. Three types of particles of the PEDOT:PSS colloidal gel—AN10, AN11, and AN13—were examined by measuring the zeta-average particle size of each sample (Figure 2). The average particle size of AN11 and AN13 PEDOT:PSS was found to be 326.9 and 382.0 nm, respectively, whereas the average particle size of AN10 PEDOT:PSS was found to be 245.6 nm. As can be seen from the size distribution of PEDOT:PSS, the particle size increased by mixing acidic and neutral PEDOT:PSS (depicted in Figure 1b). The particle size of PEDOT:PSS in water highly depends on the ratio of PEDOT to PSS. These results illustrate that neutral PEDOT:PSS has a higher PEDOT ratio in comparison to acidic PEDOT:PSS. In addition, neutral PEDOT:PSS and acidic PEDOT:PSS were found to have mixed well.

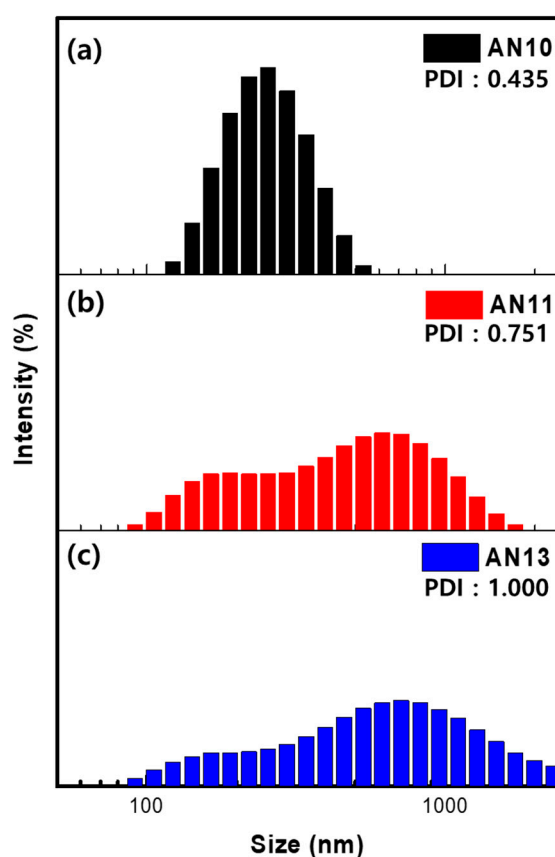


**Figure 2.** Zeta radius of samples with different ratios of acidic and neutral PEDOT:PSS. (a) AN10, (b) AN11, and (c) AN13 PEDOT:PSS.

As the gel particle polymer composite in aqueous solution is deposited and annealed forming thin PEDOT:PSS film [43,46–49], the PEDOT chains interact with the neighboring PEDOT-rich domains and bring the conducting domains closer by coalescence of PEDOT:PSS particles. The thermal annealing evaporates and softens PSS-rich domains, which improve connectivity and charge transport of conducting domains [47,50,51]. After the annealing and additional polymerization, the phase separation of PEDOT and PSS occurs. Furthermore, it increases the continuous  $\pi$ -stacking of PEDOT:PSS and provides a pathway where charge carrier can flow [37,38,52]. To identify the degree of polymerization of PEDOT and the different vibrational modes of various bonds, which are present in PEDOT:PSS layer, the spin-coated films on a silicon wafer are studied using FTIR spectroscopy (Figure 3). The FTIR spectra showed the existence of functional bonds of PEDOT:PSS after annealing at 140 °C. The typical

bands of PEDOT:PSS were observed at 1277, 1173, 1133, 1003, 966, 920, 825, and 685  $\text{cm}^{-1}$ . C–S–C bond vibrations were observed to occur at 966, 920, 825, and 685  $\text{cm}^{-1}$ . The bands at 1190 and 1003  $\text{cm}^{-1}$  were attributed to the S=O and O–S–O symmetric stretching modes in PSS, respectively. As the ratio of the neutral PEDOT:PSS increased, the peak integration at 1277  $\text{cm}^{-1}$  increased caused by the imidazole content in neutral PEDOT:PSS. Table S1 shows the peak integration and ratio of each typical band. In addition, these bands were clearly observed, which denotes that the spin-coating and annealing processes for device fabrication was carried out without degradation of the polymer.

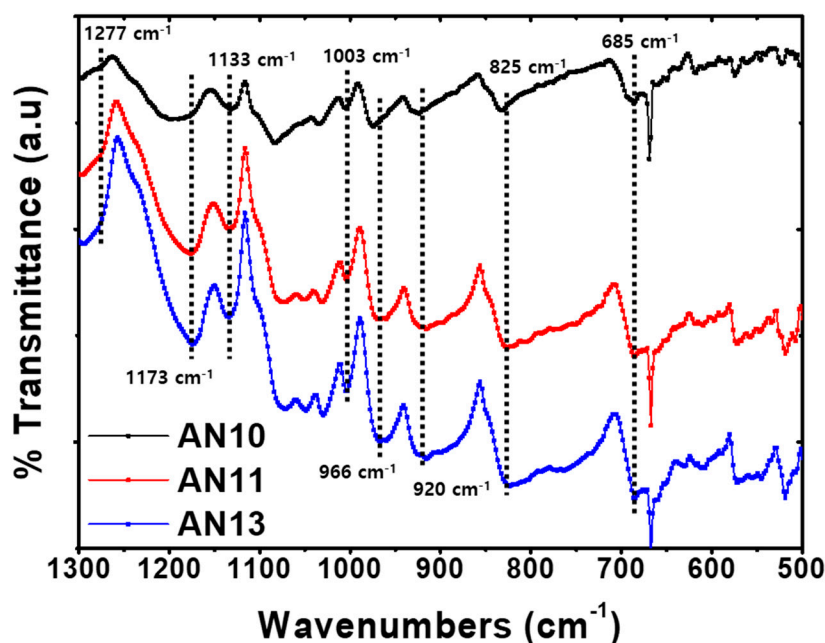


Figure 3. FTIR spectra of spin-coated AN10, AN11, and AN13 PEDOT:PSS films.

To compare the degree of electrochemical polymerization occurs at the  $\alpha, \alpha'$ -positions in polythiophene [53], the polymerization degree of PEDOT was evaluated from the ratio of integration of the infrared bands [54]. The average degree of polymerization of PEDOT can be evaluated using the equation as follows [55–57],

$$\text{Degree of polymerization} = 2\left(\frac{R_0}{R} + 2\right)$$

where R is the integrated intensity ratio of the IR bands at 685 and 825  $\text{cm}^{-1}$ , which indicates the characteristic bands of stretching vibrations of the C–S–C bond and R<sub>0</sub> is 1.07, which is determined for  $\alpha$ -sexithiophene. The films were ordered by their degree of polymerization as follows: AN11 PEDOT:PSS < AN10 PEDOT:PSS < AN13 PEDOT:PSS, indicating AN11 PEDOT:PSS exhibited the highest degree of polymerization. Thus, AN11 was found to be an efficient interlayer for PSCs with optimized PEDOT and PSS ratios and controlled pH values. For the fabrication of practicable and stable PSCs, an appropriate amount of imidazole and a high degree of polymerization is necessary. Our results indicate that the varied properties of AN10, AN11, and AN13 induce the different degree of polymerization which affects the carrier mobility of PEDOT:PSS [54,58,59]. Based on the above result, by mixing an optimized amount of neutral and acidic PEDOT:PSS, the AN11 PEDOT:PSS is expected to exhibit enhanced charge carrier mobility because of improved conjugation and polymerization with  $\pi$ - $\pi$  stacking structure which improves the electrical properties of PSCs.

The properties of mixed PEDOT:PSS such as viscosity, pH value, and colloidal gel particle size can affect the thickness and roughness of the spin-coated layer. The thickness of spin-coated PEDOT:PSS films were found to be 31–37 nm for AN10, AN11, and AN13 using the Dektak XT thickness profiler

(Figure S1). The absorbances of the films were compared (Figure S2), and those of AN11 and AN13 were similar in the visible region compared to films coated with AN10. We observed that the different properties of AN11 and AN13 did not affect the thickness and absorbance of the films. In addition, AFM topography images were obtained for different PEDOT:PSS spin-coated films (AN10, AN11, and AN13) to allow studying the possible changes in morphology at the nanometer scale (Figure 4). The root-mean-square (RMS) roughness values of AN10, AN11, and AN13 were found to be 0.28 nm, 0.32, and 0.34 nm, respectively. Furthermore, the AFM images showed a uniform and reasonably smooth surface of PEDOT:PSS film. Therefore, when different PEDOT:PSS solutions with various viscosity were mixed in a certain ratio, the thickness and surface roughness of the AN11 and AN13 films were compatible with those of the AN10 film.

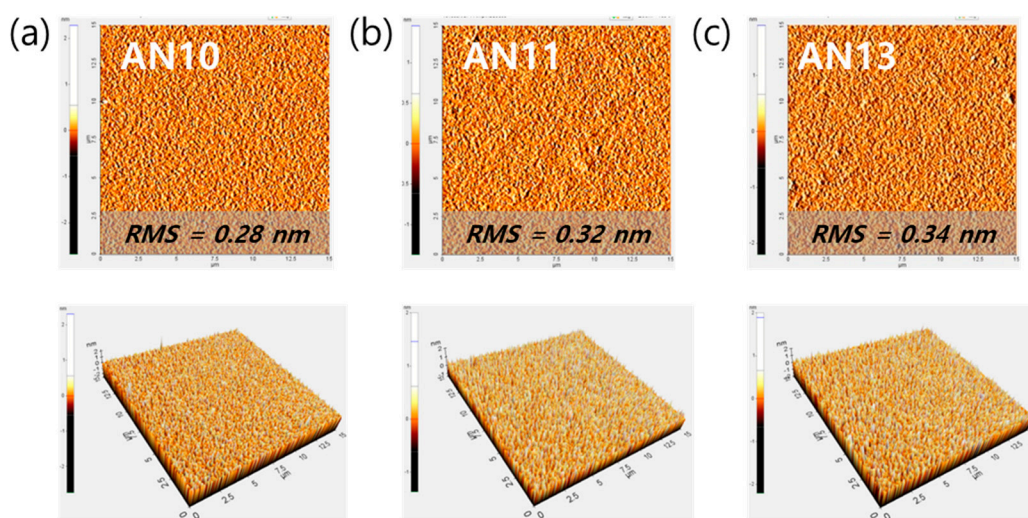


**Figure 4.** AFM topography (top) and three-dimensional views (bottom) of the surface of (a) AN10, (b) AN11, and (c) AN13 PEDOT:PSS.

Furthermore, perovskite crystals were spin-coated and analyzed for each HTL prepared by varying the volume ratios of the acidic and neutral solutions. The perovskite thin film prepared on the PEDOT:PSS layer was found to be flat, pin-hole-free, and covered the entire substrate. The perovskite film formed on the acidic PEDOT:PSS layer displayed a crystalline morphology with a perovskite crystal grain size of approximately 84 nm. As shown in Figure 5, the grain size of the AN11/perovskite film was approximately 113 nm; this result confirmed the formation of a larger grain size of the perovskite film. However, in the AN13/perovskite films, grain sizes larger than 200 nm were rarely observed, and the grain size appeared to have reduced (average 96 nm). In perovskite crystals, grain boundaries are known to provide trap sites for charges, which is disadvantageous in terms of charge transfer [60–62]. Therefore, we confirmed that AN11 samples were optimized for the smooth operation of perovskite photovoltaic cells and could also be advantageously used for perovskite crystal formation compared to AN10 and AN13.

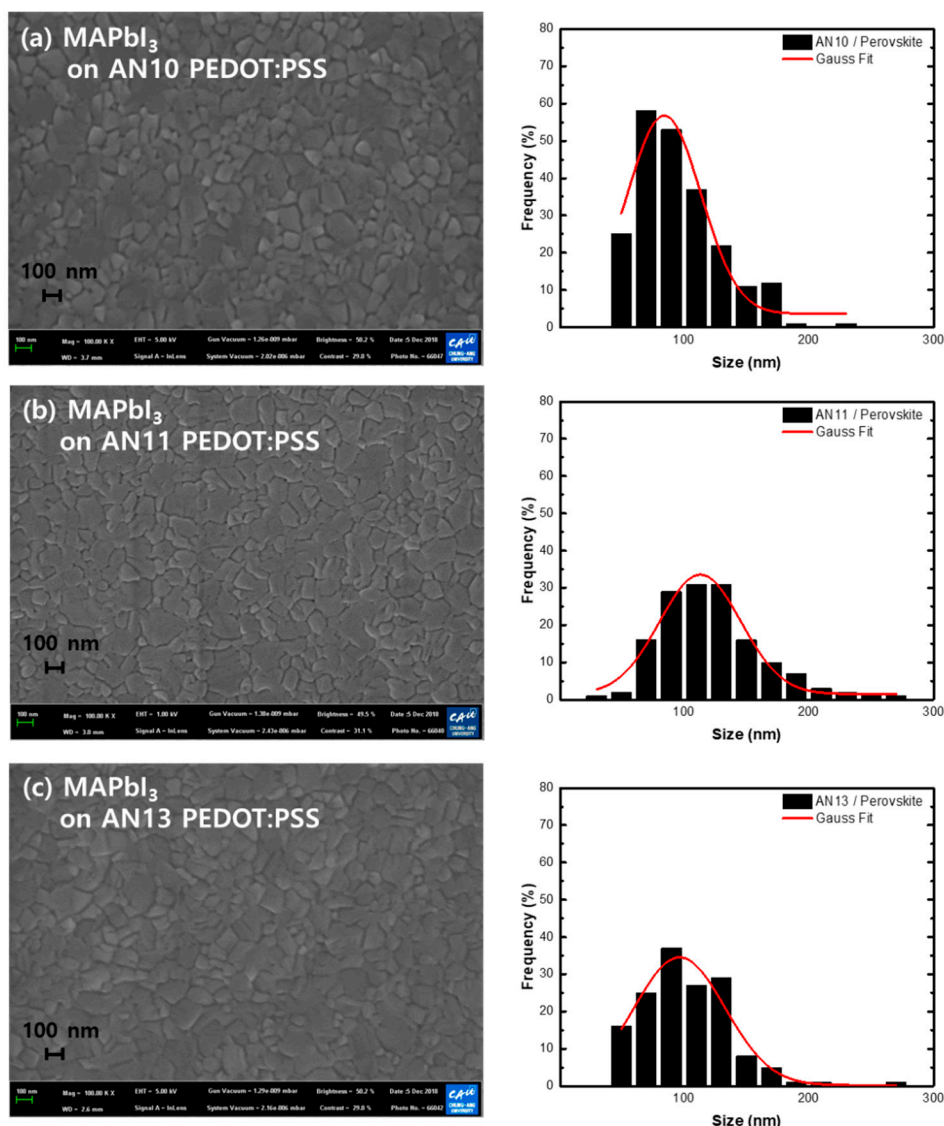


**Figure 5.** FE-SEM images of MAPbI<sub>3</sub> crystals formed on thin films with different ratios of acidic and neutral PEDOT:PSS: (a) AN10, (b) AN11, and (c) AN13.

The crystallinity of the perovskite layer is a decisive factor for device performance. To reveal the crystallinity of perovskite deposited on HTLs, X-ray diffraction (XRD) was performed, and the results are shown in Figure 6. The XRD patterns of the glass/PEDOT:PSS/MAPbI<sub>3</sub> films showed identical diffraction peaks at 14.0° (110), 28.3° (220), and 31.7° (310), which are characteristic peaks of tetragonal MAPbI<sub>3</sub> perovskite crystals. Thus, PbI<sub>2</sub> was found to completely react with CH<sub>3</sub>NH<sub>3</sub>I to form a pure perovskite phase. The full width at half maximum (FWHM) is inversely proportional to the crystal grain size, according to the Scherrer equation. The diffraction peak at 13.99° shows that the trend of FWHM is correlated with the grain size distribution of the perovskite layer in Figure 5. In addition, Figure 6a shows that the intensity of the PbI<sub>2</sub> diffraction peaks at 12.7° increased in acidic PEDOT:PSS [63–65], indicating the formation of the PbI<sub>2</sub> phase because of the acidity of PEDOT:PSS leading to degradation of perovskite. Note that the pH-controlled PEDOT:PSS induces higher perovskite crystallinity and less degradation of the perovskite layer.

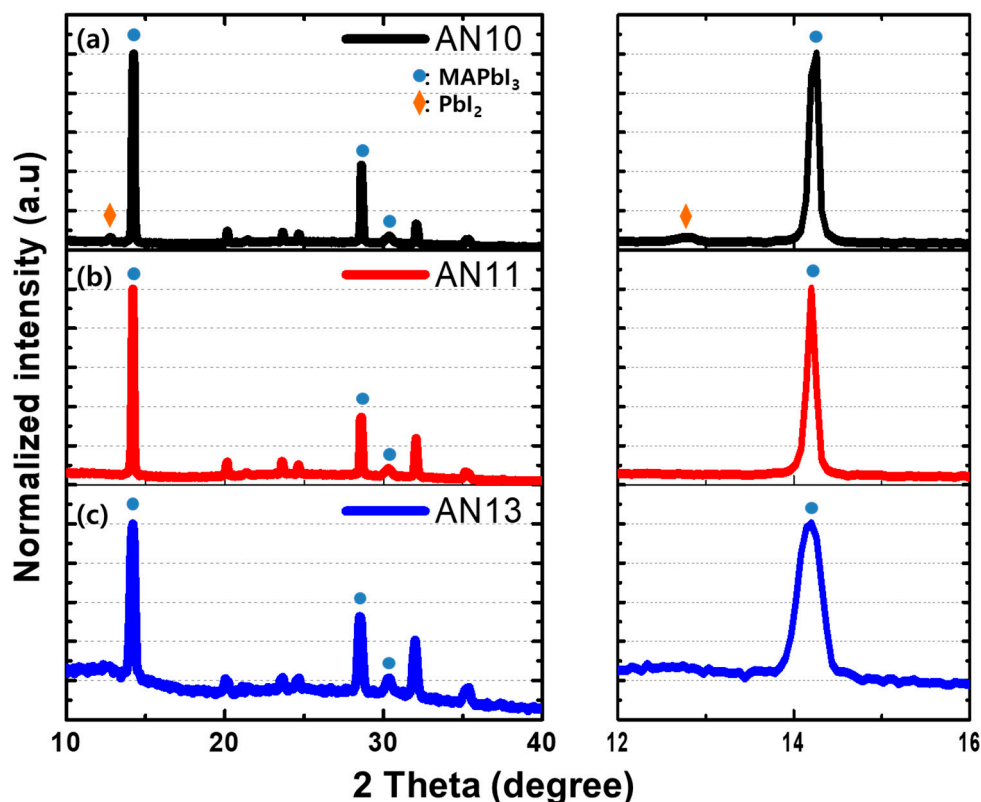


**Figure 6.** XRD patterns of the MAPbI<sub>3</sub> perovskite films on various PEDOT:PSS layers: (a) AN10, (b) AN11, and (c) AN13.

The band energy alignment and schematic structure of the PSC devices (Device structure: ITO/PEDOT:PSS/MAPbI<sub>3</sub>/PCBM/TiO<sub>x</sub>/Ag) are depicted in Figure 7a,b. Figure 7c,d shows the current-voltage (J-V) curve and the external quantum efficiency (EQE) of the PSCs manufactured using pH-modified HTLs by mixing acidic and neutral PEDOT:PSS. Table 1 shows the electrical parameters of devices based on Figure 7c,d. For PSCs fabricated with the AN10 PEDOT:PSS layer, the open-circuit voltage ( $V_{OC}$ ), short-circuit current ( $J_{SC}$ ), fill factor (FF), and power conversion efficiency (PCE) were 0.957 V, 15.28 mA cm<sup>-2</sup>, 70%, and 10.31%, respectively. Meanwhile, PSCs fabricated with the AN11 PEDOT:PSS layer exhibited increased  $V_{OC}$ , FF, and PCE values: 0.975 V, 71% and 10.34%, respectively. However, the  $J_{SC}$  value of PSCs fabricated with the AN11 PEDOT:PSS layer was similar to that of PSCs fabricated with the AN10 PEDOT:PSS layer (14.98 mA cm<sup>-2</sup>). Furthermore, the PSCs fabricated with the AN13 PEDOT:PSS layer showed an increased  $V_{OC}$  of 1.006 V but exhibited decreased  $J_{SC}$ , FF, and PCE: 13.94 mA cm<sup>-2</sup>, 68%, and 9.60%, respectively. The EQE data in Figure 7d confirm the similar  $J_{SC}$  values of the PSCs, which were 14.56, 13.69, and 12.59 mA cm<sup>-2</sup>, respectively, for the PSCs fabricated with AN10, AN11, and AN13 PEDOT:PSS layers. As the ratio of neutral PEDOT:PSS increased, the  $V_{OC}$ , measured by cyclic voltammetry, slightly increased because of the modulated work function of the PEDOT:PSS layer by mixing acidic and neutral PEDOT:PSS solutions (Figure S3). The significant decrease in the  $J_{SC}$  value with an increase of neutral PEDOT:PSS ratio can be explained by the low crystallinity of perovskite. Also, the decrease of FF and PCE in neutral PEDOT:PSS-based PSCs can be explained by low crystallinity and unsuitable morphology induced by high viscosity (Figure S4 and Table S2). PSCs with AN13 PEDOT:PSS HTLs have low  $J_{SC}$  value. In addition, FF was slightly improved in the AN11 PEDOT:PSS-based device and was the lowest in the AN13 PEDOT:PSS-based device, which can be correlated with the crystallinity and grain size of the perovskite active layer. Therefore, for the smooth and stable operation of perovskite photovoltaic cells, the optimal ratio of acidic and neutral PEDOT:PSS solutions needs to be identified. We propose an optimal ratio of acidic

to neutral PEDOT:PSS solutions of 1:1, obtained by manufacturing a device that could maintain the PCE equivalent to that of acidic PEDOT:PSS.

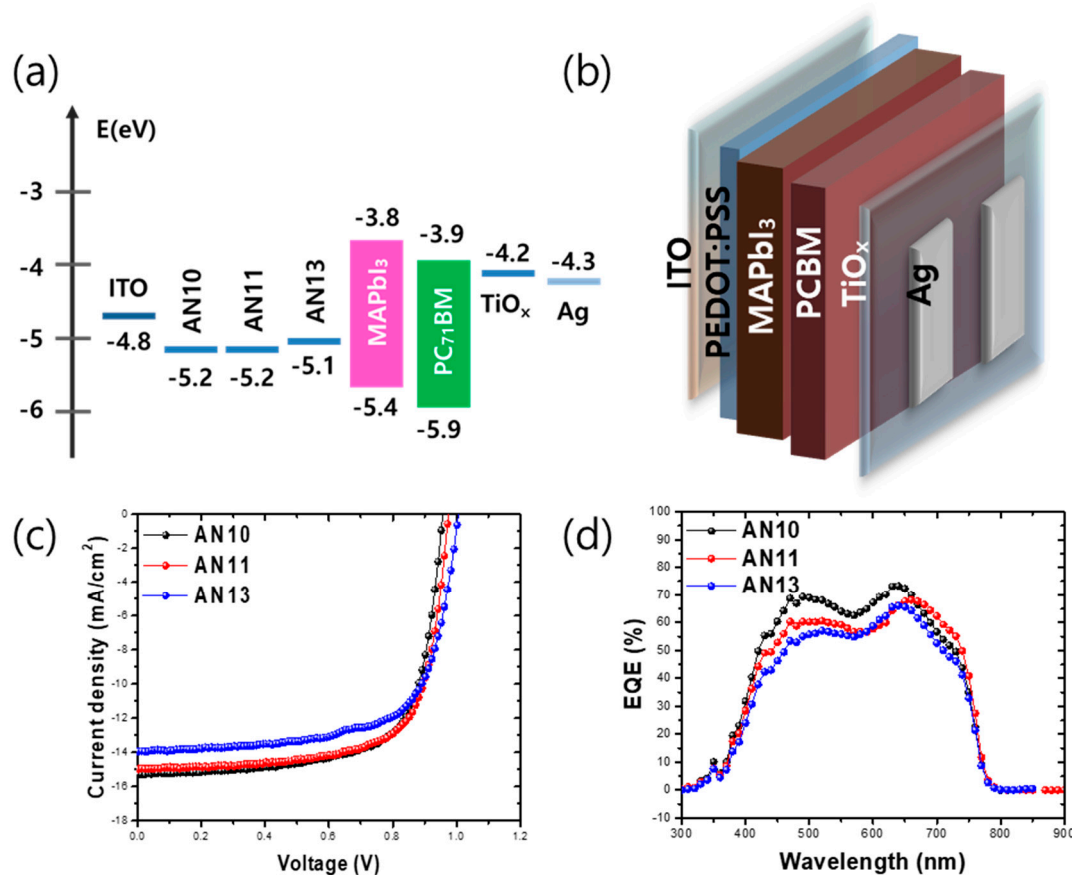


**Figure 7.** (a) Bandgap diagram of PSCs. (b) A schematic diagram of an inverted PSC. (c) Current-voltage (J–V) characteristics of PSCs under an AM 1.5 irradiation at 100 mW cm<sup>−2</sup>. (d) EQE (%) of PSCs depending on J–V characteristics.

**Table 1.** Electrical parameters of the AN10, AN11, and AN13 PEDOT:PSS-based PSCs.

Acidic: Neutral	V <sub>OC</sub> (V)	J <sub>sc</sub> (mA/cm <sup>2</sup> )	EQE (mA/cm <sup>2</sup> )	FF (%)	PCE (%)
AN10	0.957	15.28	14.56	70	10.31
AN11	0.975	14.98	13.69	71	10.34
AN13	1.006	13.94	12.59	68	9.60

Finally, stability analysis was performed to confirm the effect of improved quality and stability of PSCs. As shown in Figure 8, the effect was analyzed in a device stability test for approximately 200 h. The AN10- and AN13-based devices maintained ~80% efficiency after 50 h. However, after 50 h, the efficiency of the AN10-based devices dropped sharply, and that of the AN13-based device dropped rapidly within approximately 70 h. The increased ratio of neutral PEDOT:PSS may cause decreased stability in AN13-based PSCs because of low crystallinity and unsuitable morphology of MAPbI<sub>3</sub> perovskite. In contrast, AN11-based devices maintained 80% efficiency over 150 h. We also maintained the PCE level at 60% when the AN10- and AN13-based devices were not working. Thus, a slight increase in the PCEs compared with those of the acidic PEDOT:PSS-based device was found to be due to the improved V<sub>OC</sub> and FF and similar J<sub>SC</sub>. Furthermore, the optimized pH-controlled PEDOT:PSS was superior to acidic PESOT: PSS in terms of long-term stability of PSCs because pH-controlled PEDOT:PSS suppresses the release of indium ions in the ITO electrode and inhibits degradation of the perovskite.

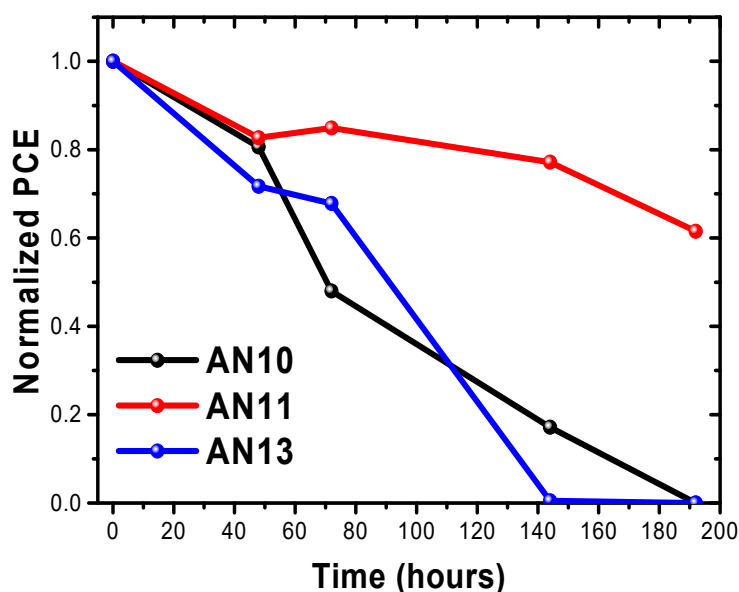


Figure 8. Long-term stability of AN10-, AN11-, and AN13-based PSCs.

#### 4. Conclusions

We suppressed the acidity of PEDOT:PSS by blending acidic and neutral PEDOT:PSS solutions at the optimal volume ratio which enhanced the stability and efficiency of PSCs. By mixing acidic and neutral PEDOT:PSS solutions, the particle size of the PEDOT:PSS colloidal gel changed, which was directly related to the ratio of PEDOT and PSS. As the ratio of neutral PEDOT:PSS increased, the acidic properties of PEDOT:PSS decreased, which enhanced the degree of polymerization. With the pH-controlled PEDOT:PSS, PSCs showed improved  $V_{OC}$  values and similar levels of  $J_{SC}$  compared with those of acidic PEDOT:PSS-based PSCs. This was achieved by better control of the PEDOT:PSS layer and the crystallization process of MAPbI<sub>3</sub> through the successful change in properties of pH-controlled HTLs. In addition, AN11 PEDOT:PSS-based devices retained 80% of the PCE in the 150-h stability test because of the improved morphological properties of the MAPbI<sub>3</sub>, whereas the PCE of PSCs fabricated with AN10 PEDOT:PSS layers fell to 20% of its initial value. Our approach for producing pH-controlled PEDOT:PSS provides a clear direction for research by providing a method to improve the stability of PSCs and can be a useful approach for solving strong acid-related problems in various conductive polymers.

**Supplementary Materials:** The following are available online at <http://www.mdpi.com/2073-4360/12/1/129/s1>, Figure S1: Thickness of spin-coated AN10-, AN11-, and AN13-PEDOT:PSS films obtained by the Dektak XT thickness profiler. Figure S2: Absorbance of the spin-coated AN10-, AN11-, and AN13-PEDOT:PSS films. Figure S3: Cyclic voltammetry (first scans) curves of AN10-, AN11-, and AN13-PEDOT:PSS films deposited onto a Pt disk electrode in Bu<sub>4</sub>NPF<sub>6</sub>/acetonitrile supporting an electrolyte/solvent system. Figure S4: (a) Current-voltage (J–V) characteristics of neutral PEDOT:PSS-based PSCs under AM 1.5 irradiation at 100 mW cm<sup>−2</sup>. (b) EQE of neutral PEDOT:PSS-based PSCs depending on J–V characteristics. Table S1: Peak integration and the ratio of various PEDOT:PSS typical bands in the FTIR spectrum. Table S2: Electrical parameters of the neutral PEDOT:PSS-based PSCs.

**Author Contributions:** Conceptualization, M.Y., and M.K.; methodology and analysis, M.Y., M.K., and W.J.; writing—original draft preparation M.K., and D.H.W.; writing—review and editing, M.K., W.J., J.K.K., and D.H.W. All authors have read and agreed to the published version of the manuscript.

**Funding:** This research was supported by the Basic Science Research Program, through the National Research Foundation of Korea (NRF), funded by the Ministry of Science, ICT, and Future Planning (2019R1F1A1041822 and 2019R1A2C1087653). This research was also supported by the Chung-Ang University Graduate Research Scholarship in 2018.

**Conflicts of Interest:** The authors declare no conflict of interest.

## References

1. Jaiswal, M.; Menon, R. Polymer electronic materials: A review of charge transport. *Polym. Int.* **2006**, *55*, 1371–1384. [[CrossRef](#)]
2. Ho, P.K.H.; Stephen, D.; Thomas; Friend, R.H.; Tessler, N. All-Polymer Optoelectronic Devices. *Science* **1999**, *285*, 233. [[CrossRef](#)] [[PubMed](#)]
3. Arias, A.C.; Granström, M.; Thomas, D.S.; Petritsch, K.; Friend, R.H. Doped conducting-polymer—Semiconducting-polymer interfaces: Their use in organic photovoltaic devices. *Phys. Rev. B* **1999**, *60*, 1854–1860. [[CrossRef](#)]
4. Gustafsson, J.C.; Liedberg, B.; Inganäs, O. In situ spectroscopic investigations of electrochromism and ion transport in a poly(3,4-ethylenedioxythiophene) electrode in a solid state electrochemical cell. *Solid State Ion.* **1994**, *69*, 145–152. [[CrossRef](#)]
5. Saghaei, J.; Fallahzadeh, A.; Yousefi, M.H. Improvement of electrical conductivity of PEDOT:PSS films by 2-Methylimidazole post treatment. *Org. Electron.* **2015**, *19*, 70–75. [[CrossRef](#)]
6. Greczynski, G.; Kugler, T.; Keil, M.; Osikowicz, W.; Fahlman, M.; Salaneck, W.R. Photoelectron spectroscopy of thin films of PEDOT–PSS conjugated polymer blend: A mini-review and some new results. *J. Electron Spectrosc. Relat. Phenom.* **2001**, *121*, 1–17. [[CrossRef](#)]
7. Kirchmeyer, S.; Reuter, K. Scientific importance, properties and growing applications of poly(3,4-ethylenedioxythiophene). *J. Mater. Chem.* **2005**, *15*, 2077–2088. [[CrossRef](#)]
8. Groenendaal, L.; Jonas, F.; Freitag, D.; Pielartzik, H.; Reynolds, J.R. Poly(3,4-ethylenedioxythiophene) and Its Derivatives: Past, Present, and Future. *Adv. Mater.* **2000**, *12*, 481–494. [[CrossRef](#)]
9. Bi, C.; Wang, Q.; Shao, Y.; Yuan, Y.; Xiao, Z.; Huang, J. Non-wetting surface-driven high-aspect-ratio crystalline grain growth for efficient hybrid perovskite solar cells. *Nat. Commun.* **2015**, *6*, 7747. [[CrossRef](#)]
10. Im, S.; Kim, W.; Cho, W.; Shin, D.; Chun, D.H.; Rhee, R.; Kim, J.K.; Yi, Y.; Park, J.H.; Kim, J.H. Improved Stability of Interfacial Energy-Level Alignment in Inverted Planar Perovskite Solar Cells. *ACS Appl. Mater. Interfaces* **2018**, *10*, 18964–18973. [[CrossRef](#)]
11. de Jong, M.P.; van Ijzendoorn, L.J.; de Voigt, M.J.A. Stability of the interface between indium-tin-oxide and poly(3,4-ethylenedioxythiophene)/poly(styrenesulfonate) in polymer light-emitting diodes. *Appl. Phys. Lett.* **2000**, *77*, 2255–2257. [[CrossRef](#)]
12. Hao, F.; Stoumpos, C.C.; Cao, D.H.; Chang, R.P.H.; Kanatzidis, M.G. Lead-free solid-state organic–inorganic halide perovskite solar cells. *Nat. Photonics* **2014**, *8*, 489–494. [[CrossRef](#)]
13. Kim, J.H.; Liang, P.-W.; Williams, S.T.; Cho, N.; Chueh, C.-C.; Glaz, M.S.; Ginger, D.S.; Jen, A.K.-Y. High-Performance and Environmentally Stable Planar Heterojunction Perovskite Solar Cells Based on a Solution-Processed Copper-Doped Nickel Oxide Hole-Transporting Layer. *Adv. Mater.* **2015**, *27*, 695–701. [[CrossRef](#)] [[PubMed](#)]
14. Zhang, F.; Johansson, M.; Andersson, M.R.; Hummelen, J.C.; Inganäs, O. Polymer Photovoltaic Cells with Conducting Polymer Anodes. *Adv. Mater.* **2002**, *14*, 662–665. [[CrossRef](#)]
15. Snaith, H.J.; Kenrick, H.; Chiesa, M.; Friend, R.H. Morphological and electronic consequences of modifications to the polymer anode ‘PEDOT:PSS’. *Polymer* **2005**, *46*, 2573–2578. [[CrossRef](#)]
16. Aernouts, T.; Vanlaeke, P.; Geens, W.; Poortmans, J.; Heremans, P.; Borghs, S.; Mertens, R.; Andriessen, R.; Leenders, L. Printable anodes for flexible organic solar cell modules. *Thin Solid Films* **2004**, *451–452*, 22–25. [[CrossRef](#)]
17. Suchand Sangeeth, C.S.; Jaiswal, M.; Menon, R. Correlation of morphology and charge transport in poly(3,4-ethylenedioxythiophene)–polystyrenesulfonic acid (PEDOT–PSS) films. *J. Phys. Condens. Matter* **2009**, *21*, 072101. [[CrossRef](#)]
18. Cao, Y.; Yu, G.; Zhang, C.; Menon, R.; Heeger, A.J. Polymer light-emitting diodes with polyethylene dioxythiophene–polystyrene sulfonate as the transparent anode. *Synth. Met.* **1997**, *87*, 171–174. [[CrossRef](#)]
19. Brown, T.M.; Kim, J.S.; Friend, R.H.; Cacialli, F.; Daik, R.; Feast, W.J. Built-in field electroabsorption spectroscopy of polymer light-emitting diodes incorporating a doped poly(3,4-ethylene dioxythiophene) hole injection layer. *Appl. Phys. Lett.* **1999**, *75*, 1679–1681. [[CrossRef](#)]
20. Ho, P.K.H.; Kim, J.-S.; Burroughes, J.H.; Becker, H.; Li, S.F.Y.; Brown, T.M.; Cacialli, F.; Friend, R.H. Molecular-scale interface engineering for polymer light-emitting diodes. *Nature* **2000**, *404*, 481–484. [[CrossRef](#)]

21. Kyaw, A.K.K.; Yemata, T.A.; Wang, X.; Lim, S.L.; Chin, W.S.; Hippalgaonkar, K.; Xu, J. Enhanced Thermoelectric Performance of PEDOT:PSS Films by Sequential Post-Treatment with Formamide. *Macromol. Mater. Eng.* **2018**, *303*, 1700429. [[CrossRef](#)]
22. Xu, S.; Hong, M.; Shi, X.-L.; Wang, Y.; Ge, L.; Bai, Y.; Wang, L.; Dargusch, M.; Zou, J.; Chen, Z.-G. High-Performance PEDOT:PSS Flexible Thermoelectric Materials and Their Devices by Triple Post-Treatments. *Chem. Mater.* **2019**, *31*, 5238–5244. [[CrossRef](#)]
23. Xue, Q.; Chen, G.; Liu, M.; Xiao, J.; Chen, Z.; Hu, Z.; Jiang, X.-F.; Zhang, B.; Huang, F.; Yang, W.; et al. Improving Film Formation and Photovoltage of Highly Efficient Inverted-Type Perovskite Solar Cells through the Incorporation of New Polymeric Hole Selective Layers. *Adv. Energy Mater.* **2016**, *6*, 1502021. [[CrossRef](#)]
24. Kim, J.-S.; Ho, P.K.H.; Murphy, C.E.; Baynes, N.; Friend, R.H. Nature of Non-emissive Black Spots in Polymer Light-Emitting Diodes by In-Situ Micro-Raman Spectroscopy. *Adv. Mater.* **2002**, *14*, 206–209. [[CrossRef](#)]
25. Chen, W.-Y.; Deng, L.-L.; Dai, S.-M.; Wang, X.; Tian, C.-B.; Zhan, X.-X.; Xie, S.-Y.; Huang, R.-B.; Zheng, L.-S. Low-cost solution-processed copper iodide as an alternative to PEDOT:PSS hole transport layer for efficient and stable inverted planar heterojunction perovskite solar cells. *J. Mater. Chem. A* **2015**, *3*, 19353–19359. [[CrossRef](#)]
26. Chen, L.-M.; Hong, Z.; Li, G.; Yang, Y. Recent Progress in Polymer Solar Cells: Manipulation of Polymer:Fullerene Morphology and the Formation of Efficient Inverted Polymer Solar Cells. *Adv. Mater.* **2009**, *21*, 1434–1449. [[CrossRef](#)]
27. Ramasami, P.; Gupta Bhowon, M.; Jhaumeer Lalloo, S.; Li Kam Wah, H. *Emerging Trends in Chemical Sciences*; Springer International Publishing AG: Cham, Switzerland, 2018; pp. 405–417.
28. Fan, P.; Zheng, D.; Zheng, Y.; Yu, J. Efficient and stable planar p-i-n perovskite solar cells by doping tungsten compound into PEDOT:PSS to facilitate perovskite crystalline. *Electrochim. Acta* **2018**, *283*, 922–930. [[CrossRef](#)]
29. Niu, Q.; Huang, W.; Tong, J.; Lv, H.; Deng, Y.; Ma, Y.; Zhao, Z.; Xia, R.; Zeng, W.; Min, Y.; et al. Understanding the mechanism of PEDOT:PSS modification via solvent on the morphology of perovskite films for efficient solar cells. *Synth. Met.* **2018**, *243*, 17–24. [[CrossRef](#)]
30. Wang, Q.; Chueh, C.C.; Eslamian, M.; Jen, A.K.Y. Modulation of PEDOT:PSS pH for efficient inverted perovskite solar cells with reduced potential loss and enhanced stability. *ACS Appl. Mater. Interfaces* **2016**, *8*, 32068–32076. [[CrossRef](#)]
31. Tsai, T.-C.; Chang, H.-C.; Chen, C.-H.; Huang, Y.-C.; Whang, W.-T. A facile dedoping approach for effectively tuning thermoelectricity and acidity of PEDOT:PSS films. *Org. Electron.* **2014**, *15*, 641–645. [[CrossRef](#)]
32. Jørgensen, M.; Norrman, K.; Gevorgyan, S.A.; Tromholt, T.; Andreasen, B.; Krebs, F.C. Stability of Polymer Solar Cells. *Adv. Mater.* **2012**, *24*, 580–612. [[CrossRef](#)] [[PubMed](#)]
33. Horii, T.; Hikawa, H.; Mochizuki, Y.; Okuzaki, H. Synthesis and Characterization of Highly Conductive PEDOT/PSS Colloidal Gels. *Trans. Mater. Res. Soc. Jpn.* **2012**, *37*, 515–518. [[CrossRef](#)]
34. McCarthy, J.E.; Hanley, C.A.; Brennan, L.J.; Lambertini, V.G.; Gun'ko, Y.K. Fabrication of highly transparent and conducting PEDOT:PSS films using a formic acid treatment. *J. Mater. Chem. C* **2014**, *2*, 764–770. [[CrossRef](#)]
35. Zhu, Z.; Liu, C.; Jiang, F.; Xu, J.; Liu, E. Effective treatment methods on PEDOT:PSS to enhance its thermoelectric performance. *Synth. Met.* **2017**, *225*, 31–40. [[CrossRef](#)]
36. Horii, T.; Li, Y.; Mori, Y.; Okuzaki, H. Correlation between the hierarchical structure and electrical conductivity of PEDOT/PSS. *Polym. J.* **2015**, *47*, 695–699. [[CrossRef](#)]
37. Alemu Mengistie, D.; Wang, P.-C.; Chu, C.-W. Effect of molecular weight of additives on the conductivity of PEDOT:PSS and efficiency for ITO-free organic solar cells. *J. Mater. Chem. A* **2013**, *1*, 9907–9915. [[CrossRef](#)]
38. Takano, T.; Masunaga, H.; Fujiwara, A.; Okuzaki, H.; Sasaki, T. PEDOT Nanocrystal in Highly Conductive PEDOT:PSS Polymer Films. *Macromolecules* **2012**, *45*, 3859–3865. [[CrossRef](#)]
39. Po, R.; Carbonera, C.; Bernardi, A.; Camaioni, N. The role of buffer layers in polymer solar cells. *Energy Environ. Sci.* **2011**, *4*, 285–310. [[CrossRef](#)]
40. Rider, D.A.; Harris, K.D.; Wang, D.; Bruce, J.; Fleischauer, M.D.; Tucker, R.T.; Brett, M.J.; Buriak, J.M. Thienylsilane-Modified Indium Tin Oxide as an Anodic Interface in Polymer/Fullerene Solar Cells. *ACS Appl. Mater. Interfaces* **2009**, *1*, 279–288. [[CrossRef](#)]

41. Choi, H.; Mai, C.-K.; Kim, H.-B.; Jeong, J.; Song, S.; Bazan, G.C.; Kim, J.Y.; Heeger, A.J. Conjugated polyelectrolyte hole transport layer for inverted-type perovskite solar cells. *Nat. Commun.* **2015**, *6*, 7348. [[CrossRef](#)]
42. Crispin, X.; Jakobsson, F.L.E.; Crispin, A.; Grim, P.C.M.; Andersson, P.; Volodin, A.; van Haesendonck, C.; Van der Auweraer, M.; Salaneck, W.R.; Berggren, M. The Origin of the High Conductivity of Poly(3,4-ethylenedioxythiophene)–Poly(styrenesulfonate) (PEDOT–PSS) Plastic Electrodes. *Chem. Mater.* **2006**, *18*, 4354–4360. [[CrossRef](#)]
43. Lang, U.; Müller, E.; Naujoks, N.; Dual, J. Microscopical Investigations of PEDOT:PSS Thin Films. *Adv. Funct. Mater.* **2009**, *19*, 1215–1220. [[CrossRef](#)]
44. Wu, X.; Liu, J.; Wu, D.; Zhao, Y.; Shi, X.; Wang, J.; Huang, S.; He, G. Highly conductive and uniform graphene oxide modified PEDOT:PSS electrodes for ITO-free organic light emitting diodes. *J. Mater. Chem. C* **2014**, *2*, 4044–4050. [[CrossRef](#)]
45. Zhang, B.; Tan, G.; Lam, C.-S.; Yao, B.; Ho, C.-L.; Liu, L.; Xie, Z.; Wong, W.-Y.; Ding, J.; Wang, L. High-Efficiency Single Emissive Layer White Organic Light-Emitting Diodes Based on Solution-Processed Dendritic Host and New Orange-Emitting Iridium Complex. *Adv. Mater.* **2012**, *24*, 1873–1877. [[CrossRef](#)]
46. Yeo, J.-S.; Yun, J.-M.; Kim, D.-Y.; Park, S.; Kim, S.-S.; Yoon, M.-H.; Kim, T.-W.; Na, S.-I. Significant Vertical Phase Separation in Solvent-Vapor-Annealed Poly(3,4-ethylenedioxythiophene):Poly(styrene sulfonate) Composite Films Leading to Better Conductivity and Work Function for High-Performance Indium Tin Oxide-Free Optoelectronics. *ACS Appl. Mater. Interfaces* **2012**, *4*, 2551–2560. [[CrossRef](#)]
47. Nardes, A.M.; Kemerink, M.; Janssen, R.A.J.; Bastiaansen, J.A.M.; Kiggen, N.M.M.; Langeveld, B.M.W.; van Breemen, A.J.J.M.; de Kok, M.M. Microscopic Understanding of the Anisotropic Conductivity of PEDOT:PSS Thin Films. *Adv. Mater.* **2007**, *19*, 1196–1200. [[CrossRef](#)]
48. Skotheim, T.A.; Reynolds, J. *Conjugated Polymers: Processing and Applications*; CRC Press: Boca Raton, FL, USA, 2006.
49. Vitoratos, E.; Sakkopoulos, S.; Dalas, E.; Paliatsas, N.; Karageorgopoulos, D.; Petraki, F.; Kennou, S.; Choulis, S.A. Thermal degradation mechanisms of PEDOT:PSS. *Org. Electron.* **2009**, *10*, 61–66. [[CrossRef](#)]
50. Fan, X.; Nie, W.; Tsai, H.; Wang, N.; Huang, H.; Cheng, Y.; Wen, R.; Ma, L.; Yan, F.; Xia, Y. PEDOT:PSS for Flexible and Stretchable Electronics: Modifications, Strategies, and Applications. *Adv. Sci.* **2019**, *6*, 1900813. [[CrossRef](#)]
51. Kemerink, M.; Timpanaro, S.; de Kok, M.M.; Meulenkaamp, E.A.; Touwslager, F.J. Three-Dimensional Inhomogeneities in PEDOT:PSS Films. *J. Phys. Chem. B* **2004**, *108*, 18820–18825. [[CrossRef](#)]
52. Nardes, A.M.; Janssen, R.A.J.; Kemerink, M. A Morphological Model for the Solvent-Enhanced Conductivity of PEDOT:PSS Thin Films. *Adv. Funct. Mater.* **2008**, *18*, 865–871. [[CrossRef](#)]
53. Zhang, D.; Qin, J.; Xue, G. An investigation of the electropolymerization of terthiophene in boron fluoride–ethyl ether. *Synth. Met.* **1999**, *100*, 285–289. [[CrossRef](#)]
54. Olivares, A.J.; Cosme, I.; Sanchez-Vergara, M.E.; Mansurova, S.; Carrillo, J.C.; Martinez, H.E.; Itzmoyotl, A. Nanostructural Modification of PEDOT:PSS for High Charge Carrier Collection in Hybrid Frontal Interface of Solar Cells. *Polymers* **2019**, *11*, 1034. [[CrossRef](#)] [[PubMed](#)]
55. Aradilla, D.; Casanovas, J.; Estrany, F.; Iribarren, J.I.; Alemán, C. New insights into the characterization of poly(3-chlorothiophene) for electrochromic devices. *Polym. Chem.* **2012**, *3*, 436–449. [[CrossRef](#)]
56. Zhao, Q.; Jamal, R.; Zhang, L.; Wang, M.; Abdiryim, T. The structure and properties of PEDOT synthesized by template-free solution method. *Nanoscale Res. Lett.* **2014**, *9*, 557. [[CrossRef](#)]
57. Geetha, S.; Trivedi, D.C. A new route to synthesize high degree polythiophene in a room temperature melt medium. *Synth. Met.* **2005**, *155*, 232–239. [[CrossRef](#)]
58. Shi, H.; Liu, C.; Xu, J.; Song, H.; Lu, B.; Jiang, F.; Zhou, W.; Zhang, G.; Jiang, Q. Facile Fabrication of PEDOT:PSS/Polythiophenes Bilayered Nanofilms on Pure Organic Electrodes and Their Thermoelectric Performance. *ACS Appl. Mater. Interfaces* **2013**, *5*, 12811–12819. [[CrossRef](#)]
59. Shi, H.; Liu, C.; Jiang, Q.; Xu, J. Effective Approaches to Improve the Electrical Conductivity of PEDOT:PSS: A Review. *Adv. Electron. Mater.* **2015**, *1*, 1–16. [[CrossRef](#)]
60. Park, J.-S.; Calbo, J.; Jung, Y.-K.; Whalley, L.D.; Walsh, A. Accumulation of Deep Traps at Grain Boundaries in Halide Perovskites. *ACS Energy Lett.* **2019**, *4*, 1321–1327. [[CrossRef](#)]

61. Xie, F.; Chen, C.-C.; Wu, Y.; Li, X.; Cai, M.; Liu, X.; Yang, X.; Han, L. Vertical recrystallization for highly efficient and stable formamidinium-based inverted-structure perovskite solar cells. *Energy Environ. Sci.* **2017**, *10*, 1942–1949. [[CrossRef](#)]
62. Ying, X.; Liu, Y.; Ling, L.; Xu, M.; Bao, B.; Bao, X.; Pang, A.; Shao, G.; Zhang, Y.; Fang, J.-K. Low-Cost, High-Efficiency, and Efficiency Predictable Small Molecule Organic Dyes with Bis(4-styryl)phenyl Amino Donor for Dye-Sensitized Solar Cells. *Sol. RRL* **2019**, *3*, 1970061. [[CrossRef](#)]
63. Brenner, T.M.; Rakita, Y.; Orr, Y.; Klein, E.; Feldman, I.; Elbaum, M.; Cahen, D.; Hodes, G. Conversion of Single Crystalline PbI<sub>2</sub> to CH<sub>3</sub>NH<sub>3</sub>PbI<sub>3</sub>: Structural Relations and Transformation Dynamics. *Chem. Mater.* **2016**, *28*, 6501–6510. [[CrossRef](#)]
64. Zhang, H.; Tao, M.; Gao, B.; Chen, W.; Li, Q.; Xu, Q.; Dong, S. Preparation of CH<sub>3</sub>NH<sub>3</sub>PbI<sub>3</sub> thin films with tens of micrometer scale at high temperature. *Sci. Rep.* **2017**, *7*, 8458. [[CrossRef](#)] [[PubMed](#)]
65. Shirayama, M.; Kato, M.; Miyadera, T.; Sugita, T.; Fujiseki, T.; Hara, S.; Kadowaki, H.; Murata, D.; Chikamatsu, M.; Fujiwara, H. Degradation mechanism of CH<sub>3</sub>NH<sub>3</sub>PbI<sub>3</sub> perovskite materials upon exposure to humid air. *J. Appl. Phys.* **2016**, *119*, 115501. [[CrossRef](#)]



© 2020 by the authors. Licensee MDPI, Basel, Switzerland. This article is an open access article distributed under the terms and conditions of the Creative Commons Attribution (CC BY) license (<http://creativecommons.org/licenses/by/4.0/>).